Supporting Information

Hybrid Composites of Quantum Dots, Monolayer WSe_2, and Ag Nanodisks for White Light–Emitting Diodes

Chiao-Yun Chang[1], Cheng-Li Yu[1], Chen-An Lin[1,2], Hsiang-Ting Lin[1], Andrew Boyi Lee[1], Zheng-Zhe Chen[1], Li-Syuan Lu[3], Wen-Hao Chang[3], Hao-Chung Kuo[2], and Min-Hsiung Shih[1,2,4,*]

[1] Research Center for Applied Sciences (RCAS), Academia Sinica
128 Academia Road, Section 2, Nangang, Taipei 11529, Taiwan, ROC.
[2] Department of Photonics, National Chiao Tung University
1001 University Road, Hsinchu 30010, Taiwan, ROC.
[3] Department of Electrophysics, National Chiao Tung University
1001 University Road, Hsinchu 30010, Taiwan, ROC.
[4] Department of Photonics, National Sun Yat-sen University, 70 Lianhai Road, Gushan District, Kaohsiung 804201, Taiwan, ROC.

[*]Email:mhshih@gate.sinica.edu.tw

S1. The structural characterization of QD-Ag-WSe_2 structure

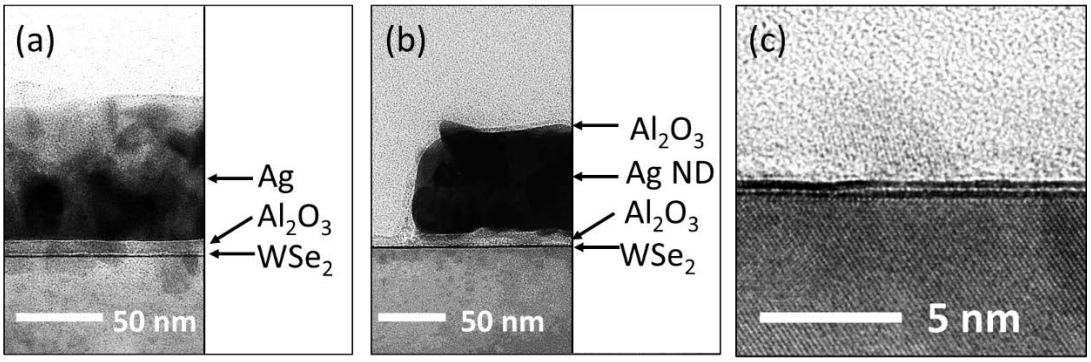

Figure S1 (a) The cross-sectional transmission electron microscopy (TEM) image of Ag thin film on the 5.0 ± 0.3 nm Al_2O_3/monolayer WSe_2/SiO_2 substrate. (b) The cross-sectional TEM image of Ag ND with coating the 5.0 ± 1.5 nm Al_2O_3 thin film on the Al_2O_3/monolayer WSe_2/SiO_2 substrate. (c) The cross–sectional TEM image of monolayer WSe_2 in the hybrid nanostructure.

The transmission electron microscopy (TEM) images of QD-Ag-WSe_2 structure specifically for the Al_2O_3 spacer layer and monolayer WSe_2 show in the Figure S1. Figure S1 (a) is a Ag thin film deposited on a Al_2O_3/WSe_2/ SiO_2 substrate. It can be seen that the thickness of the Al_2O_3 layer is about 5.0 ± 0.3 nm. Figure S1 (b) is a TEM image of the Ag ND with coated the Al_2O_3 thin film on the Al_2O_3/WSe_2/SiO_2 substrate. It can be confirmed that the Al_2O_3 thin film have a perfectly coating on the surface of Ag ND and can be observed that the thickness of the Al_2O_3 thin film is not

uniform. The thickness of Al_2O_3 is estimated approximately 5.0 ± 1.5 nm.

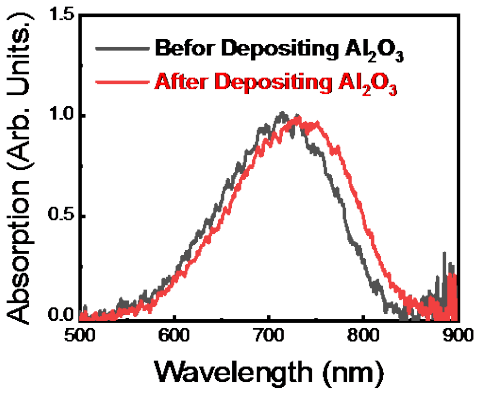

Figure S2. Absorption spectra of a Ag ND with a diameter of 210 nm before and after depositing the Al_2O_3 layer.

Absorption spectra of Ag NDs in the QD-Ag-WSe_2 structure before and after depositing an Al_2O_3 thin film on the top of to characterize the optical properties of LSPR for a Ag ND as shown in Figure S2. The absorption spectrum of the Ag ND after covered with an Al_2O_3 layer only slightly redshifts due to the small change of the surrounding dielectric medium.

S2. The optical properties of Ag NDs with varying the diameter of disks

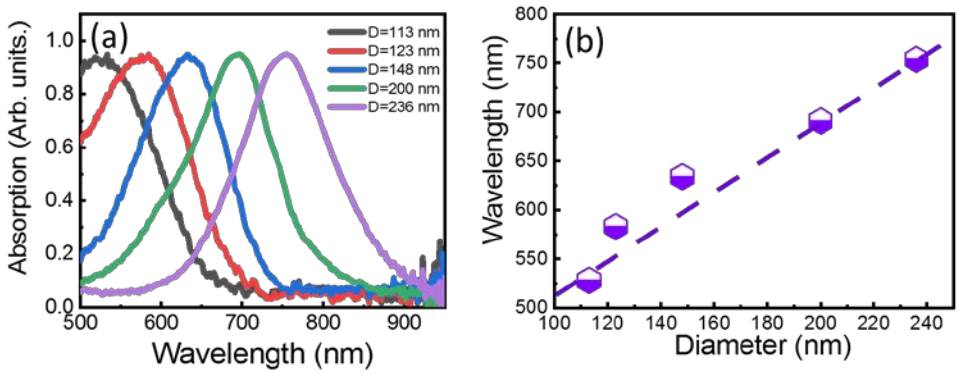

Figure S3 (a) Absorption spectra of Ag NDs with varying the diameter of the Ag ND from 113 to 236 nm. (b) Absorption peak of Ag NDs as a function of the diameter of the Ag ND.

Figure S3 is the optical properties of Ag NDs with varying the diameter of Ag NDs from 113 to 236 nm. The resonant wavelength of Ag NDs gradually increase with increasing the diameter of the Ag ND. The average full width half maximum (FWHM) of absorption spectra for all Ag NDs are approximately 128.0 ± 3.5 nm.

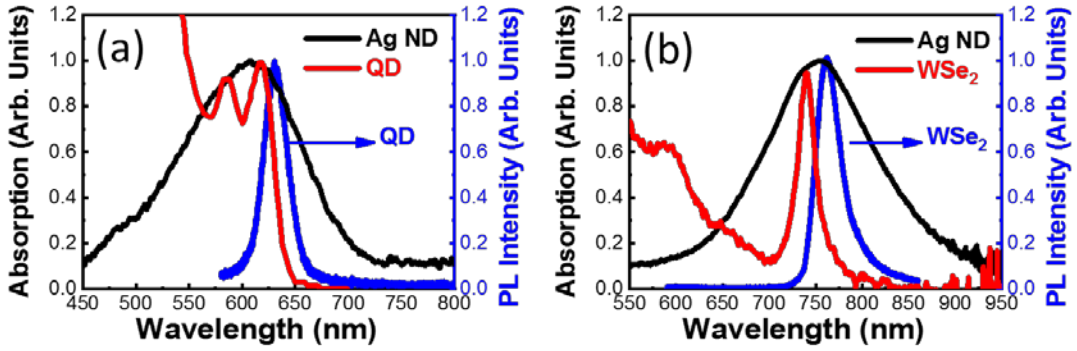

Figure S4. (a) Absorption spectra of core–shell CdSe/CdS quantum dot (QD) and the Ag ND with a diameter of 123 nm. And the photoluminescence (PL) spectrum of CdSe/CdS QDs. (c) Absorption spectra of monolayer WSe_2 and the Ag ND with a diameter of 240 nm. And the photoluminescence (PL) spectrum of WSe_2.

The localized surface plason resonance (LSPR) of a Ag ND at the resonant wavelength of 600 nm perfectly overlaps with the emission and absorption spectrum of QDs as shown in Figure S4 (a). The LSPR of a Ag ND at the resonant wavelength of 750 nm perfectly overlaps with the emission and absorption spectrum of monolayer WSe_2 as shown in Figure S4 (b)

S3. The time-resolve photoluminescence (TRPL) analysis

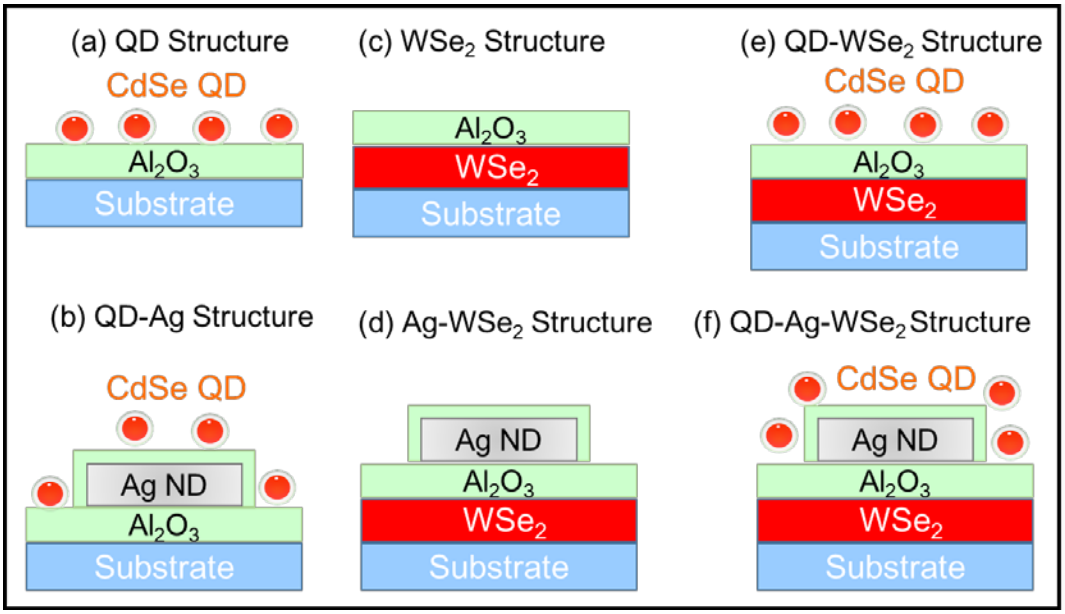

Figure S5 The schematic of (a) QD structure, (b) QD-Ag structure, (c) WSe_2 structure, (d) Ag-WSe_2 structure, (e) QD-WSe_2 structure, and (f) QD-Ag-WSe_2 structure.

In order to understand the energy transfer efficiency from bare QD to ML WSe_2, the PL spectra and TRPL curve of QD and ML WSe_2 in the QD, WSe_2, and QD-WSe_2 structures show in the Figure S6. It can be see that both the PL intensity of QD and WSe_2 in the QD-WSe_2 structure are slight quenching, which imply that there nearly is no the energy transfer from the QDs to ML WSe_2 emission in this structure. In the following equations, the equation S(1) is the PL decay curve of QD emission as a function of time. The τ is the PL lifetime of QD. Those curves were reasonably fitted by a tri-exponential decay descripted in the equation (1). The PL lifetime of τ_1, τ_2, and τ_3 for CdSe QD are attributed the fast component of the charged exciton, the slow component of the band-edge excitons, and the non-radiative component of the deep-level traps, respective.[1] The PL decay rate (K) of QD peak shows in the equation S(2). The PL lifetime of QD in the QDand QD-WSe_2 structures are listed in table S1. The non-radiative component of QD-WSe_2 structure have obvious change. The relationships of the PL decay rates ($K_{QD-WSe2}$) of CdSe QD in the QD-WSe_2 structures are listed in the equation S(3). The K_{QD} is only the total spontaneous emission rate of bare CdSe QD. The decay rate of $K_{inf,\ QD-WSe_2}$ could be caused by the interface interaction between the exciton of QD and the exciton of WSe_2 to form the non-radiative component. The $K_{inf,\ QD-WSe_2}$ is near 0.02 ns^{-1}. Therefore, we confirm that there is no the energy conversion between QD and WSe_2 and partial QD carriers in the QD-WSe_2 structure are consumed to slightly decrease the PL intensity of QD.

Structure	τ_1 (ns)	τ_2 (ns)	τ_3 (ns)	K (ns^{-1})
QD	1.26 $\pm$0.05	6.41$\pm$0.22	21.78$\pm$1.66	0.99$\pm$0.03
QD-WSe_2	1.26$\pm$0.06	6.49$\pm$0.23	17.26$\pm$1.09	1.01$\pm$0.03

Table S1. The PL lifetime of QD in the QD and QD-WSe_2 structures.

$$\mathrm{I}(t) = A_1 e^{\frac{-t}{\tau_1}} + A_2 e^{\frac{-t}{\tau_2}} + A_3 e^{\frac{-t}{\tau_3}} \quad \text{.....S (1)}$$

$$K = \frac{1}{\tau_1} + \frac{1}{\tau_2} + \frac{1}{\tau_3} \quad \text{.....S (2)}$$

$$K_{QD-WSe_2} = K_{QD} + K_{inf,\ QD-WSe_2} \text{.....S (3)}$$

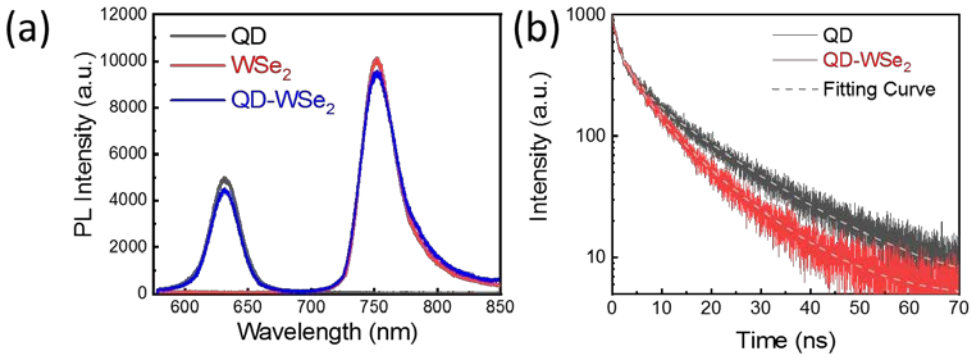

Figure S6 (a) PL spectra of QDs and WSe_2 in the QD, WSe_2, and QD-WSe_2 structures. (b) PL decay curves of QDs emission in the QD and QD-WSe_2 structures.

PL decay curves of QD in the QD-Ag and QD-Ag-WSe_2 structures with varying the absorption wavelength of Ag NDs are shown in Figure S7. PL lifetimes of QDs in the QD-Ag and QD-Ag-WSe_2 structures with varying the absorption wavelength of Ag NDs were estimated by using a tri-exponential decay fitting as shown in the Figure S8. It can be see that τ_1 and τ_2 in the QD-Ag and QD-Ag-WSe_2 structures obviously change with varying the absorption wavelength of Ag NDs, which indicates that the QD-Ag and QD-Ag-WSe_2 structures exist plasmon-exiton interactions.

The relationships of the PL decay rates (K) of CdSe QDs in three structures are listed in the equation R(4) to R(6). The $K_1(\lambda)$, $K_2(\lambda)$, and $K_3(\lambda)$ are the PL decay rate of QDs in the QD, QD-Ag, and QD-Ag-WSe_2 structures, respectively. The $K_2(\lambda)$, $K_3(\lambda)$, and $K_3(\lambda) - K_2(\lambda)$ as a function of the absorption wavelength of a Ag ND show in the Figure S9. The K_1 of the QD structure is only the total spontaneous emission rate ($K_{QD} = 0.99 \pm 0.03$ ns^{-1}) of bare CdSe QD.

It can be seen that the $K_2(\lambda)$ of the QD-Ag structure is dependent on the absorption wavelength of Ag NDs because the coupling rate ($K_{c,\ QD-Ag}(\lambda)$) between QDs and a Ag ND is newly added in this structure from plasmon-exciton coupling effect. The absorption wavelength of Ag ND at 600 nm has the optimal value of $K_2(\lambda)$ due to the perfect overlapping with the absorption spectrum of a Ag ND and the emission spectrum of CdSe QDs. The values of $K_{c,\ QD-Ag}(\lambda)$ at the wavelengths of 500 nm and 850 nm are almost a constant, which means that the absorption peak of Ag ND is far away from the absorption and emission peaks of QD, and there are almost independent on the plasmon-exciton coupling effect. The trend of $K_2(\lambda)$ curve is consistent with the results of PL enhancement in the QD-Ag structure.

Compared with the QD-Ag structure, the value of the $K_3(\lambda)$ in the QD-Ag-WSe_2 structure is significantly increased and the full width at half maximum of $K_3(\lambda)$ curve becomes more broad. The $K_3(\lambda)$-$K_2(\lambda)$ at 500 and 850 nm are almost a

constant and the experimental color conversion efficiency at 500 and 850 nm are also approximately zero. It implies that QD carriers could be partly influenced in the QD-Ag ND-WSe_2 structure to form the additional decay rate $K_{inf,\ QD-Ag-WSe_2}$ of the interface interaction. The $K_{inf,\ QD-Ag-WSe_2}$ can be estimated approximately 0.4 ns^{-1}. Then, the transfer rate ($K_{ET}(\lambda)$) can be calculated by $K_{ET}(\lambda) = K_3(\lambda)$-$K_2(\lambda)$-$K_{inf,\ QD-Ag-WSe_2}$. The $K_{ET}(\lambda)$ curve shows in the Figure S10. The trend of $K_{ET}(\lambda)$ curve is similar with the results of color conversion efficiency from QD to WSe_2 emission with varying the absorption wavelength of a Ag ND. The maximum value of K_{ET}=0.16 ns^{-1} is at a plasmon resonance of 650 nm. . Figure S10 (b) shows the fitting and normalized curves of the QD EF in the QD-Ag structure, the WSe_2 EF in the Ag-WSe_2 structure, and the color conversion efficiency. It is worth mentioning that the maximum value of experimental color conversion efficiency is at a plasmon resonance of 650 nm and near the intersection of the QD EF and WSe_2 EF curves.

$K_1 = K_{QD}$ ……R (4)

$K_2(\lambda) = K_{QD} + K_{c,\ QD-Ag}(\lambda)$……R (5)

$K_3(\lambda) = K_{QD} + K_{c,\ QD-Ag}(\lambda) + K_{ET}(\lambda) + K_{inf,\ QD-Ag-WSe_2}$ ……R (6)

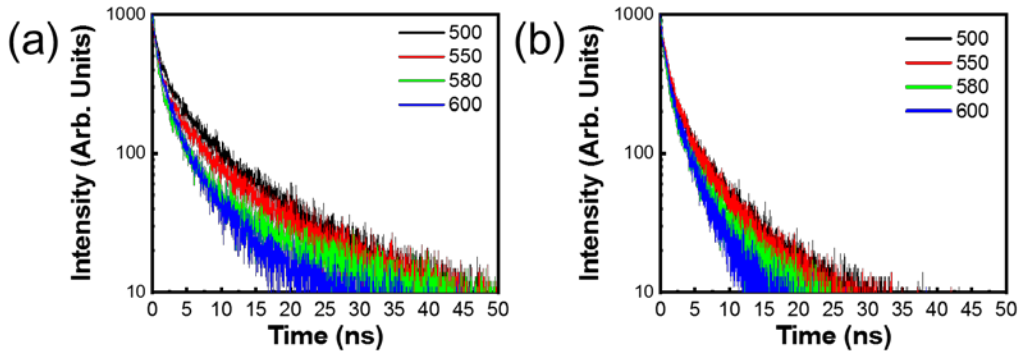

Figure S7 (a) PL decay curves of CdSe QDs peak in the QD–Ag structure with varying the absorption wavelength of Ag NDs from 500 to 600 nm. (b) PL decay curves of CdSe QDs peak in the QD–Ag-WSe_2 structure with varying the absorption wavelength of Ag NDs from 500 to 600 nm.

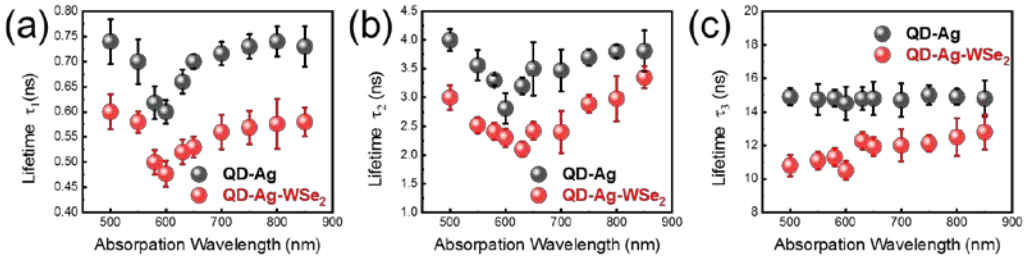

Figure S8 (a) The τ_1 of CdSe QDs in the QD–Ag and QD–Ag-WSe_2 structures as a function of the plasmon resonance wavelength of a Ag NDs. (b) The τ_2 of CdSe QDs in the QD–Ag and QD–Ag-WSe_2 structures as a function of the plasmon resonance wavelength of a Ag NDs. (c) The τ_3 of CdSe QDs in the QD–Ag and QD–Ag-WSe_2 structures as a function of the plasmon resonance wavelength of a Ag NDs.

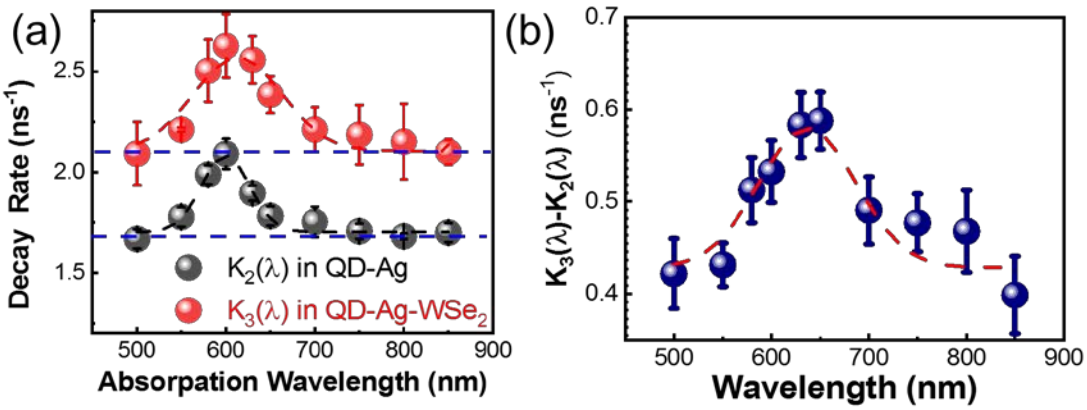

Figure S9 (a) PL decay rates of QDs in the QD–Ag and QD–Ag-WSe_2 structures as a function of the plasmon resonance wavelength of a Ag NDs. (b) $K_3(\lambda)$-$K_2(\lambda)$ of QDs in the QD–Ag and QD–Ag-WSe_2 structures as a function of the plasmon resonance wavelength of a Ag NDs.

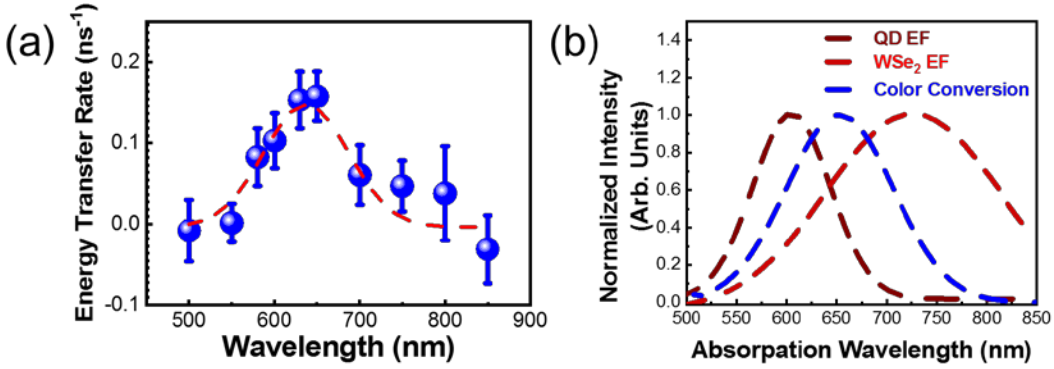

Figure S10 (a) Energy transfer rates of QDs in the QD–Ag and QD–Ag-WSe_2 structures as a function of the plasmon resonance wavelength of a Ag NDs. (b) The normalized fitting curve of QD enhancement (EF), WSe_2 EF, and color conversion efficiency as a function of absorption wavelength of Ag NDs.

Reference

1. Mehata, M. S.; Ratnesh, R. K. Luminescence properties and exciton dynamics of core-multi-shell semiconductor quantum dots leading to QLEDs. *Dalton. Trans.* **2019,** *48*, 7619-7631.